Journal of Power Sources 196 (2011) 1717–1722

Contents lists available at ScienceDirect

Journal of Power Sources

journal homepage: www.elsevier.com/locate/jpowsour

Non-precious metal catalysts synthesized from precursors of carbon, nitrogen, and transition metal for oxygen reduction in alkaline fuel cells

Xuguang Li [a], Branko N. Popov [a,*], Takeo Kawahara [b], Hiroyuki Yanagi [b]

[a] Center for Electrochemical Engineering, Department of Chemical Engineering, University of South Carolina, Columbia, SC 29208, USA
[b] Corporate Development Dept., Tokuyama Corporation, Wadai 40, Tsukuba, Ibaraki 300-4247, Japan

ARTICLE INFO

Article history:
Received 4 August 2010
Received in revised form 4 October 2010
Accepted 5 October 2010
Available online 14 October 2010

Keywords:
Non-precious metal catalyst
Alkaline fuel cell
Oxygen reduction
Anion exchange membrane

ABSTRACT

Non-precious metal catalysts (NPMCs) synthesized from the precursors of carbon, nitrogen, and transition metals were investigated as an alternate cathode catalyst for alkaline fuel cells (AFCs). The procedures to synthesize the catalyst and the post-treatment were tailored to refine its electrocatalytic properties for oxygen reduction reaction (ORR) in alkaline electrolyte. The results indicated that the performance of NPMCs prepared with carbon-supported ethylenediamine-transition metal composite precursor and subjected to heat-treatment shows comparable activity for oxygen reduction with Pt/C catalyst. The NPMC exhibits an open circuit potential of 0.97 V and a maximum power density of 177 mW cm^{-2} at 50 °C when tested in anion exchange membrane (AEM) fuel cells.

1. Introduction

The alkaline fuel cells (AFCs) have advantages over the polymer electrolyte membrane (PEM) fuel cells due to less corrosive environment and more facile kinetics for oxygen reduction reaction (ORR). However, a serious CO_2 poisoning problem hinders the development of the AFCs usually using a liquid electrolyte such as potassium hydroxide (KOH) aqueous solution. The CO_2 contained in the oxidant gas stream reacts with the OH^- ion to produce the carbonate (CO_3^{2-}) and bicarbonate (HCO_3^-). The carbonate, i.e., K_2CO_3 reduces the ionic conductivity of the electrolyte and blocks the pores in the electrode. Recently, with the development of anion exchange membrane (AEM) as solid electrolyte in AFCs (similar to PEM fuel cells), the cell may be potentially simplified and CO_2 poisoning problem is alleviated due to the lack of mobile cation in the membrane. Thus, recently a renaissance in the AFCs is occurring [1–3].

Non-precious metal catalysts (NPMCs) have been extensively studied as a low-cost catalyst alternative to Pt for the ORR in acid medium in PEM fuel cells in the past four decades [4–34]. However, the active sites of the NPMCs in acid medium are still a subject of controversy. The main difference between two viewpoints is the role of transition metal playing in the catalysts, while nitrogen is believed to be a part of active sites. The conventional hypothesis is the metal-N_4/N_2 moiety bound to carbon substrate is an active site for oxygen reduction [9]. A newly developed hypothesis is that the graphitic and pyridinic nitrogen doped on the carbon substrate's surface plays an important role toward the ORR. The transition metal primarily serves to facilitate the incorporation of nitrogen into the graphitic carbon during the pyrolysis. The remaining metal particles are encased in the carbon substrate [10–14].

In the past seven years, our group has systematically studied the activity and stability, as well as the nature of active sites of NPMCs for the ORR [15–24]. The highly active NPMCs have been prepared by subjecting carbon-supported nitrogen-metal chelates or nitrogen-containing organic compound-modified carbon black to a treatment combination of pyrolysis, leaching, and re-pyrolysis. According to our studies [15–24] and those reported by other researchers in the literature [12–14], the pyridinic-N and graphitic-N are believed to play important roles in the active sites of NPMCs. The pyridinic-N is a type of nitrogen that bonds to two carbon atoms in the carbon plane with a basic lone pair of electrons. Since the lone pair of electrons is not delocalized into the aromatic π-system, the pyridinic-N can be protonated to form a pyridinic-N-H (a pyridinium) in the acid electrolyte, which was demonstrated by our research group by XPS analysis of the catalysts before and after fuel cell stability test.

The transition of pyridinic-N to pyridinic-N-H is responsible for the initial fast performance degradation of NPMC-based fuel cells. As expected, our preliminary work indicated that the NPMC has much higher activity and stability for the ORR in alkaline electrolyte than in acidic electrolyte [23].

* Corresponding author at: Department of Chemical Engineering, University of South Carolina, Swearingen Engineering Building, 301 Main Street, Columbia, SC 29208, USA. Tel.: +1 803 777 7314; fax: +1 803 777 8265.
E-mail address: popov@cec.sc.edu (B.N. Popov).

0378-7753/$ – see front matter © 2010 Elsevier B.V. All rights reserved.
doi:10.1016/j.jpowsour.2010.10.018

In this work, the influence of compositions of catalysts and the post-treatment methods on the activity of NPMCs in alkaline electrolyte was studied using rotating disk electrode (RDE) technique. The fuel cell performance of the optimal non-noble metal catalyst was studied using AEM fuel cell.

2. Experimental

2.1. Preparation of non-precious metal catalysts

The non-precious metal catalysts were synthesized according to a revised procedure [24]. Briefly, 2 mL of ethylenediamine (EDA, $NH_2CH_2CH_2NH_2$) was added to a 8.5 mM of $Co(NO_3)_2$ and 8.5 mM of $FeSO_4$ solution (the nominal atomic ratio of Co:Fe is 1:1), followed by the addition of carbon black (Ketjenblack®, EC300J). The reaction mixture was refluxed at 85 °C for 4 h and then dried using a rotary evaporator at 80 °C under reduced pressure. The dried sample (denoted as CoFeN/C) was heated to 900 °C under an argon atmosphere for 2 h (denoted as CoFeN/C-H). The heat-treated sample was leached in 0.5 M H_2SO_4 at 80 °C to remove excess metals on the surface of the catalyst (denoted as CoFeN/C-HL). The resulting samples were filtered, washed, and then heat-treated again at 900 °C under an argon atmosphere for 2 h (denoted as CoFeN/C-HLH).

For comparison, the catalysts prepared with carbon-supported EDA without and with heat-treatment are denoted as N/C and N/C-H. The catalysts prepared with carbon-supported $Co(NO_3)_2$ and $FeSO_4$ without and with heat-treatment are denoted as CoFe/C and CoFe/C-H.

2.2. Rotating disk electrode measurements

RDE measurements were performed in a standard three-compartment electrochemical cell. A glassy carbon disk (5.61 mm diameter) was used as the working electrode. Mercury/mercury oxide (Hg/HgO) was used as the reference electrode in alkaline electrolyte, while platinum foil was used as the counter electrode. A 0.1 M KOH was used as the electrolyte. This condition is commonly used to study the catalytic properties of catalysts for oxygen reduction on RDE in alkaline solution [35–37]. All potentials in this work are referenced to a reversible hydrogen electrode (RHE). The catalyst ink was prepared by mixing 24 mg of the catalyst with 3 mL of isopropyl alcohol. Next, 15 μL of the ink was deposited onto the glassy carbon and left to dry at room temperature. The electrode was scanned in N_2-saturated electrolyte at a sweep rate of 5 mV s^{-1} to evaluate the background capacitance current. Linear sweep voltammograms in O_2-saturated electrolyte were measured at 900 rpm. The oxygen reduction current was determined as the difference between currents measured in the N_2- and O_2-saturated electrolytes.

2.3. Fuel cell testing

The cathode catalyst ink was prepared by blending the catalyst with AS-4 anion exchange resin solution (5 wt%, Tokuyama) and isopropyl alcohol. The catalyst ink was sprayed onto a gas diffusion layer (SGL Carbon 10 BC, Germany) until a catalyst loading of 4 mg cm^{-2} was achieved. For comparison, a cathode with a Pt loading of 0.4 mg cm^{-2} (TKK 46% Pt/C) was also prepared. The anode Pt loading is 0.4 mg cm^{-2}. The anode and cathode were hot-pressed to an A201 anion exchange membrane (Tokuyama Corporation, Japan) at 140 °C. The membrane is composed of hydrocarbon type main chain and quaternary ammonium groups as ion exchange site (thickness: 28 μm; ion-exchange capacity: 1.8 mmol g^{-1}; OH^- conductivity: 42 mS cm^{-1}). The geometric area of the membrane and electrode (MEA) was 5 cm^{-2}.

Pure H_2 gas and O_2 humidified at 50 °C were supplied to the anode and cathode compartments, respectively. The flow rates of H_2 and O_2 were 200 and 400 mL min^{-1}, respectively. Polarization experiments were conducted using a fully automated test station (Fuel Cell Technologies Inc.) at 50 °C according to the test protocol suggested by the supplier of anion exchange membrane, Tokuyama Corporation.

3. Results and discussion

Fig. 1a shows the polarization curves for oxygen reduction on N/C, CoFe/C, and CoFeN/C catalysts. The measurements were conducted in O_2-saturated 0.1 M KOH using a potential scan rate of 5 mV s^{-1} and an electrode rotation rate of 900 rpm. The performance of carbon is presented for comparison. As shown in Fig. 1a in alkaline electrolyte, all samples, even bare carbon, are catalytically active toward oxygen reduction. All catalysts show a steep reduction current between 0.8 and 0.6 V. Additionally, the onset potential of the ORR on carbon is as high as 0.808 V. A slight activity decrease is observed for the N/C catalyst after the deposition of ethylenediamine (EDA) on carbon black, with an onset potential of 0.786 V. The addition of cobalt and iron salts onto carbon black makes a positive shift of the onset potential of CoFe/C catalyst to 0.839 V, indicating Co and Fe species are active for oxygen reduction. When Co- and Fe-EDA chelates are supported on carbon, the resultant CoFeN/C exhibits the highest activity. In fact, the transition metal chelates are superior to the corresponding metal ions alone for catalyzing oxygen reduction in alkaline electrolyte. Fig. 1b shows the Tafel plots on N/C, CoFe/C, and CoFeN deduced from Fig. 1a. The kinetic current density, i_k, is estimated by correcting the mass transport according to equation (1) [35]:

$$i_{\text{kin}} = \frac{i_l i}{i_l - i} \quad (1)$$

where i_l is the limiting current density, and i is the measured current density. As shown in Fig. 1b, the electrocatalytic activity difference of the catalysts can be clearly identified in the low current density region. For clarity, Table 1 summarizes the onset potentials (obtained from Fig. 1a) and the potentials measured at a kinetic current density of 1.0 mA cm^{-2} (obtained from Fig. 1b) of oxygen reduction on different catalysts. It is evident that the activity of catalysts without post-treatment decreases in the order: CoFeN/C > CoFe/C > Carbon > N/C.

Fig. 1c shows the cyclic voltammograms for N/C, CoFe/C, and CoFeN/C catalysts. The measurements were conducted in N_2-saturated 0.1 M KOH using a potential scan rate of 50 mV s^{-1}. The carbon exhibits higher capacitance current with a pair of redox peaks at 0.4–0.5 V, attributing to the quinone/hydroquinone redox system. After the deposition of EDA, Co and Fe salts, or Co- and

Table 1
Onset potentials (obtained from polarization curves) and the potentials measured at a kinetic current density of 1.0 mA cm^{-2} (obtained from Tafel plots) of oxygen reduction on different catalysts measured by RDE.

Catalysts		Onset potential (V)	Potential at 1.0 mA cm^{-2} (V)
Without post treatment	Carbon	0.808	0.731
	N/C	0.786	0.714
	CoFe/C	0.839	0.747
	CoFeN/C	0.839	0.775
Heat-treatment	N/C-H	0.842	0.767
	CoFe/C-H	0.842	0.767
	CoFeN/C-H	0.938	0.827
Other treatments	CoFeN/C-HL	0.948	0.827
	CoFeN/C-HLH	0.948	0.842
	Pt/C	0.989	0.862

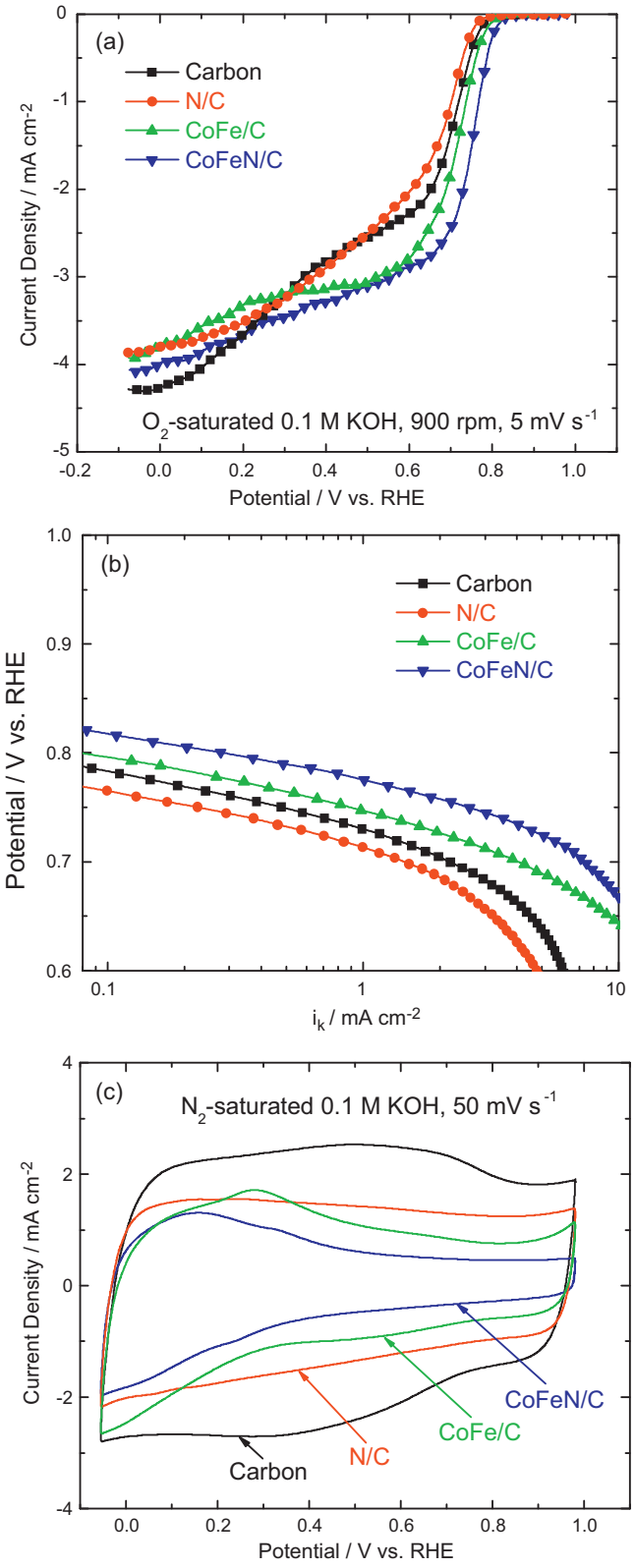

Fig. 1. (a) Polarization curves for the oxygen reduction reaction in O_2-saturated 0.1 M KOH on N/C, CoFe/C, and CoFeN. The carbon is presented for comparison. Scan rate: 5 mV s^{-1}; rotation rate: 900 rpm. (b) Tafel plots on N/C, CoFe/C, and CoFeN deduced from the polarization curves in (a). (c) The cyclic voltammograms of N/C, CoFe/C, and CoFeN in N_2-saturated 0.1 M KOH. The carbon is presented for comparison. Scan rate: 50 mV s^{-1}.

Fe-EDA composites, the capacitance current of the corresponding N/C, CoFe/C, and CoFeN/C gradually decreases. This is due to the blockage of pores of carbon black, which results in a decrease of the surface area of carbon [38]. A pair of redox peaks was observed for CoFe/C, CoFeN/C at 0.2–0.3 V and 0–0.1 V, respectively due to the presence of metal-containing species in the catalysts.

Fig. 2a shows the polarization curves for oxygen reduction on the heat-treated catalysts of N/C-H, CoFe/C-H, and CoFeN/C-H. The measurements were conducted in O_2-saturated 0.1 M KOH using a potential scan rate of 5 mV s^{-1} and an electrode rotation rate of 900 rpm. Compared to the non-treated counterparts shown in Fig. 1a, the activity of N/C-H and CoFeN/C-H was greatly improved demonstrated by the observed positive shift of 56 mV and 99 mV for the onset potentials. Fig. 2b shows the Tafel plots on the heat-treated catalysts of N/C-H, CoFe/C-H, and CoFeN/C-H deduced from Fig. 2a. At kinetic current density of 1.0 mA cm^{-2}, the potential increase is up to 53 and 52 mV for N/C-H and CoFeN/C-H, respectively, while it is about 20 mV for CoFe/C-H. A well-defined limiting current plateau is observed for CoFeN/C-H in Fig. 2a. According to the results shown in Fig. 2a and b and Table 1, the activity of the heat-treated catalysts decreases in the order: CoFeN/C-H $\gg$ CoFe/C-H $\approx$ N/C-H. Therefore, the CoFeN/C catalysts were selected for further performance optimization studies.

Fig. 2c shows the cyclic voltammograms for the heat-treated catalysts of N/C-H, CoFe/C-H, and CoFeN/C-H. The measurements were conducted in N_2-saturated 0.1 M KOH using a potential scan rate of 50 mV s^{-1}. No characteristic redox peak is observed for N/C-H. Both CoFe/C-H and CoFeN/C-H exhibit a pair of redox peaks at 0.2–0.3 V and 0–0.1 V from the metal-containing species. Therefore, higher activity of CoFeN/C-H over CoFe/C-H shown in Fig. 2a and b can be attributed to the presence of the active N-containing species in the former, which is pyridinic-N and graphitic-N demonstrated by XPS analysis in our previous studies [17,19,23]. The activity increase of heat-treated N/C-H compared to N/C (see Figs. 1a and b and 2a and b) is explained as the incorporation of active N-containing sites into carbon substrate resulting from high-temperature heat-treatment [19]. This process is accelerated by the presence of transition metals [11–13,17].

Fig. 3a shows the polarization curves for oxygen reduction on the CoFeN/C catalysts treated under different conditions. The measurements were conducted in O_2-saturated 0.1 M KOH using a potential scan rate of 5 mV s^{-1} and an electrode rotation rate of 900 rpm. It is evident that the catalysts subject to pyrolysis and the combination of pyrolysis and leaching exhibit very similar catalytic performance toward oxygen reduction. A re-pyrolysis further slightly increases the activity of catalysts. This tendency is clearly demonstrated by the Tafel plots for oxygen reduction on CoFeN/C-H, CoFeN/C-HL, and CoFeN/C-HLH in Fig. 3b.

Fig. 3c shows the cyclic voltammograms for CoFeN/C catalysts treated under different conditions. The measurements were conducted in N_2-saturated 0.1 M KOH using a potential scan rate of 50 mV s^{-1}. Subject to the acid-leaching, the peaks related to the metal-containing species at 0–0.3 V in CoFeN/C-H are not observed for CoFeN/C-HL and CoFeN/C-HLH. In consideration of high activity of CoFeN/C-HL and especially CoFeN/C-HLH shown in Fig. 3a, it can be concluded that, the N-containing species on carbon is part of the active sites for the ORR.

Fig. 4 shows the performance comparison of CoFeN/C-HLH and Pt/C catalysts for oxygen reduction in O_2-saturated 0.1 M KOH including the ring currents, the numbers of electron exchanged during oxygen reduction, polarization curves, and the Tafel plots. The data of carbon black is also presented for comparison. The ring currents were measured on Pt ring electrode held at 1.2 V for CoFeN/C-HLH and Pt/C catalysts. As shown in Fig. 4a, it is evident that the ring currents for CoFeN/C-HLH and Pt/C are comparable. In contrast, the ring current for carbon is much higher. The number of

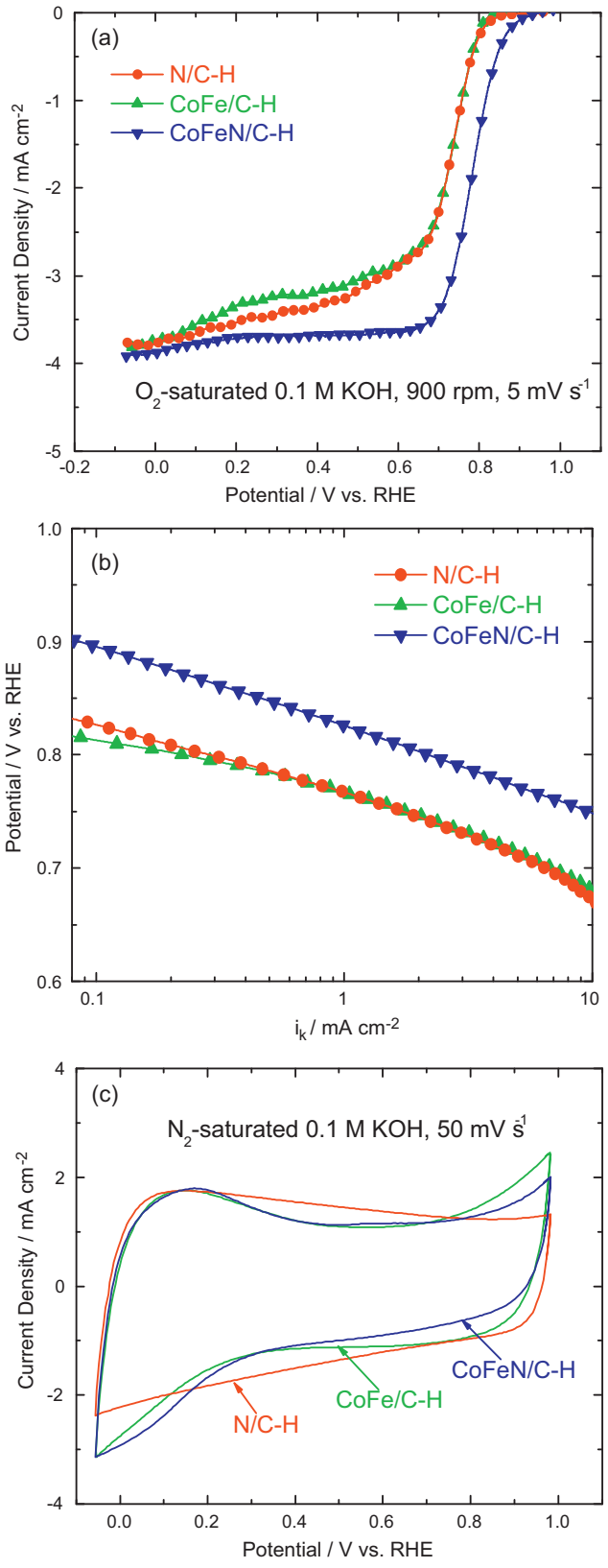

Fig. 2. (a) Polarization curves for the oxygen reduction reaction in O_2-saturated 0.1 M KOH on the heat-treated catalysts of N/C-H, CoFe/C-H, and CoFeN/C-H. Scan rate: 5 mV s^{-1}; rotation rate: 900 rpm. (b) Tafel plots on the heat-treated catalysts of N/C-H, CoFe/C-H, and CoFeN/C-H deduced from the polarization curves in (a). (c) Cyclic voltammograms of the heat-treated catalysts of N/C-H, CoFe/C-H, and CoFeN/C-H in N_2-saturated 0.1 M KOH. Scan rate: 50 mV s^{-1}.

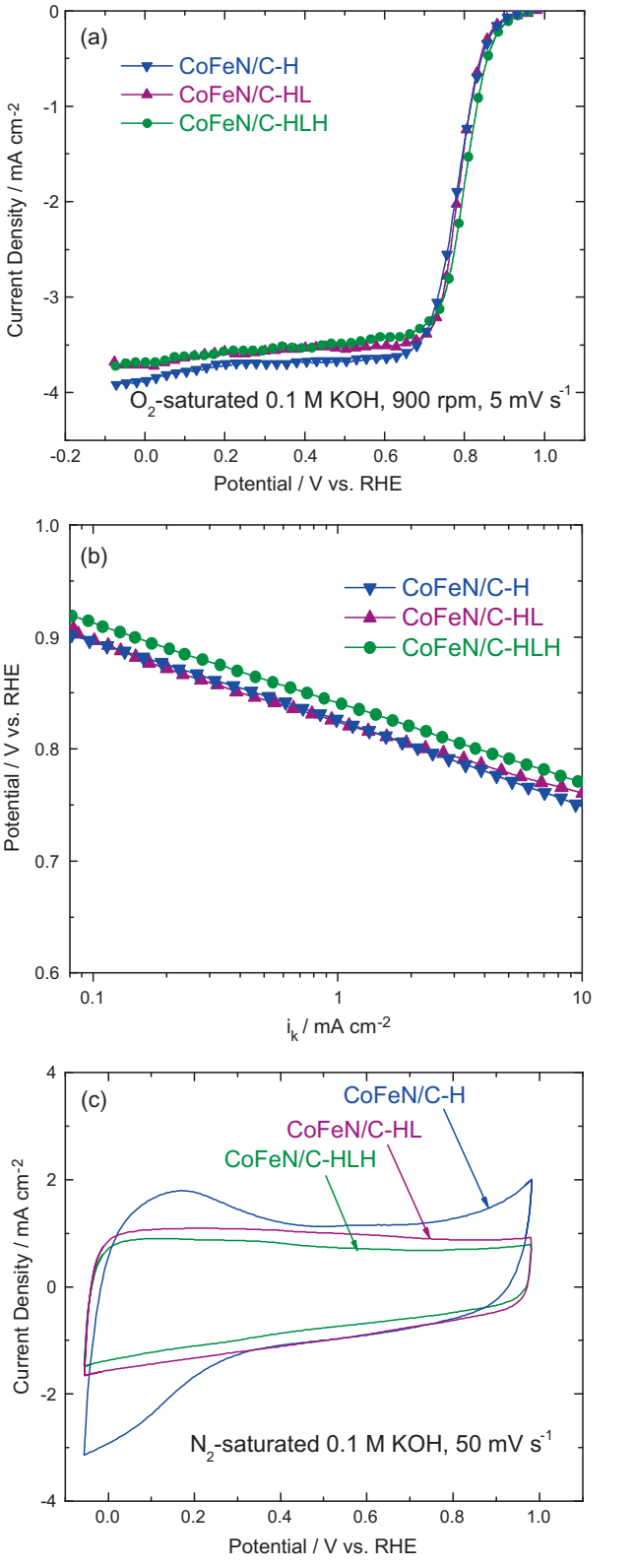

Fig. 3. (a) Polarization curves for the oxygen reduction reaction in O_2-saturated 0.1 M KOH on the CoFeN/C catalysts treated under different conditions: CoFeN/C-H, CoFeN/C-HL, and CoFeN/C-HLH. The Pt/C catalyst is presented for comparison. Scan rate: 5 mV s^{-1}; rotation rate: 900 rpm. (b) Tafel plots on the CoFeN/C catalysts treated under different conditions: CoFeN/C-H, CoFeN/C-HL, and CoFeN/C-HLH deduced from the polarization curves in (a). (c) Cyclic voltammograms in N_2-saturated 0.1 M KOH for the CoFeN/C catalysts treated under different conditions: CoFeN/C-H, CoFeN/C-HL, and CoFeN/C-HLH. The Pt/C catalyst is presented for comparison. Scan rate: 50 mV s^{-1}.

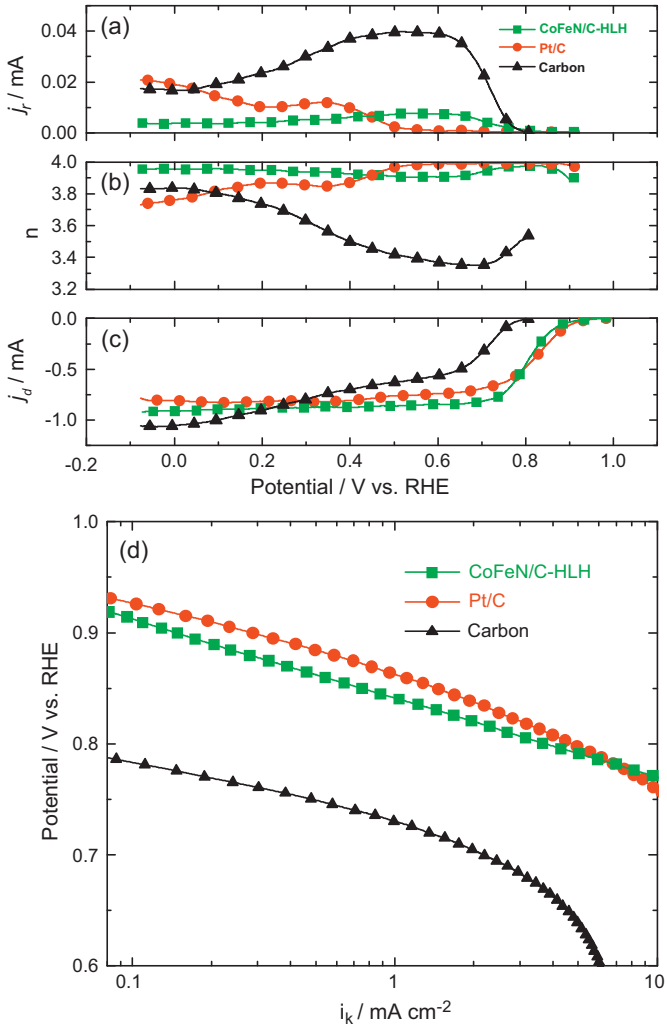

Fig. 4. Comparison of CoFeN/C-HLH and Pt/C catalysts for the oxygen reduction reaction in O_2-saturated 0.1 M KOH. Scan rate: 5 mV s^{-1}; rotation rate: 900 rpm. (a) Ring currents; (b) the number of electron exchanged during oxygen reduction; (c) polarization curves; (d) Tafel plots deduced from the polarization curves in (c). The data of carbon black is also presented for comparison.

electron exchanged (n) during oxygen reduction can be calculated by the following equation [15]:

$$n = \frac{4j_d}{j_d + (j_r/N)} \quad (2)$$

where j_d is the disk current, j_r is the ring current and $N = 0.37$ is the RRDE collection efficiency. The n for CoFeN/C-HLH and Pt/C is shown in Fig. 4b, which is about 3.9–4.0 at high potential. This indicates that both CoFeN/C-HLH and Pt/C catalysts catalyze the ORR mainly via a four-electron pathway in alkaline electrolyte. For carbon black alone, a lower selectivity with n of about 3.3–3.6 was observed at high potential. Combined with the polarization curves and Tafel plots shown in Fig. 4c and d, it can be concluded that the catalytic performance of CoFeN/C-HLH is very comparable with Pt/C for oxygen reduction in alkaline electrolyte, which is much higher than carbon black alone.

Fig. 5 shows the preliminary performance of a H_2–O_2 anion exchange membrane fuel cell. The operation temperature is 50 °C. The Pt loading at anode is 0.4 mg cm^{-2}, whereas the catalyst loadings at cathode are 4 mg cm^{-2} for CoFeN/C-HLH and 0.4 mg$_{Pt}$ cm^{-2} for Pt/C. Anode and cathode gases are humidified at 50 °C. The flow rates of H_2 and O_2 are 200 and 400 mL min^{-1}. The open circuit potentials are 0.97 and 1.04 V for CoFeN/C-HLH and Pt/C,

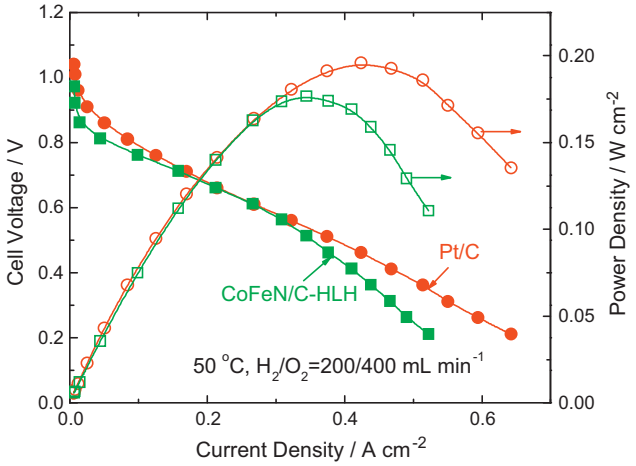

Fig. 5. Preliminary performance of a H_2–O_2 anion exchange membrane fuel cell. The operation temperature is 50 °C. The Pt loading at anode is 0.4 mg cm^{-2}, whereas the catalyst loadings at cathode are 4 mg cm^{-2} for CoFeN/C-HLH and 0.4 mg$_{Pt}$ cm^{-2} for Pt/C. Anode and cathode gases are humidified at 50 °C. The flow rates of H_2 and O_2 are 200 and 400 mL min^{-1}.

respectively. This trend is in good agreement with the RDE results shown in Table 1. The maximum power densities are 177 and 196 mW cm^{-2} for CoFeN/C-HLH and Pt/C, respectively. At high potential, the performance of CoFeN/C-HLH is slightly lower than Pt/C. At intermediate potential, they show very similar performance. The lower performance of CoFeN/C-HLH over Pt/C at low potential may be attributed to higher mass-transfer resistance of the former resulting from higher catalyst loading and thus higher thickness of catalyst layer.

Activity issues aside, the stability of catalysts is another crucial parameter to determine their applicability in a practical fuel cell. In our preliminary potential cycling stability test on RDE, the optimal non-precious metal catalyst is demonstrated to be exceptionally stable in alkaline electrolyte due to the nature of active sites in the catalysts [23] and less corrosive alkaline environment [1,2]. The optimization studies of the performance of CoFeN/C-HLH-based MEAs are in progress. A long-term stability of NPMCs in AEM fuel cell will be carried out in the future.

4. Conclusions

The influence of the compositions of non-precious metal catalysts (NPMCs) and the post-treatment methods on the performance of catalysts for oxygen reduction in alkaline electrolyte is investigated by RDE technique. The Co- and Fe-N-based precursors are found to be superior to the single nitrogen or metal salt precursors. The heat-treatment plays a crucial role in generating highly active catalytic sites. The nitrogen-containing species, such as pyridinic-N and graphitic-N are the active sites of NPMC. The CoFeN/C treated by the combination of pyrolysis, leaching, and re-pyrolysis exhibit very comparable activity with Pt/C catalyst. The preliminary H_2–O_2 anion exchange membrane fuel cell tests demonstrate a maximum power density of 177 mW cm^{-2} and open circuit potential (OCP) of 0.97 V for CoFeN/C-HLH. For Pt/C catalyst, the maximum power density and the OCP are 196 mW cm^{-2} and 1.04 V, respectively.

Acknowledgements

The financial support of the Department of Energy (contract no. DE-FG36-08GO88116) and National Science Foundation (contract no. 0966956) is acknowledged gratefully.

References

[1] F. Bidault, D.J.L. Brett, P.H. Middleton, N.P. Brandon, J. Power Sources 187 (2009) 39–48.
[2] E. Antolini, E.R. Gonzalez, J. Power Sources 195 (2010) 3431–3450.
[3] M. Ni, M.K.H. Leung, D.Y.C. Leung, Proceedings of 16th World Hydrogen Energy Conference (WHEC 16), Lyon, France, 13–16 June, 2006.
[4] R. Jasinski, Nature 201 (1964) 1212–1213.
[5] H. Jahnke, M. Schönbron, G. Zimmermann, Top. Curr. Chem. 61 (1976) 133–181.
[6] V.S. Bogatzky, M.R. Tarasevich, K.A. Radyushkina, O.E. Levina, S.I. Andrusyova, J. Power Sources 2 (1977) 233–240.
[7] J.A.R. van Veen, H.A. Colijn, Ber. Bunsenges. Phys. Chem. 85 (1981) 700–704.
[8] S.L. Gupta, D. Tryk, I. Bae, W. Aldred, E.B. Yeager, J. Appl. Electrochem. 19 (1989) 19–27.
[9] M. Lefèvre, E. Proietti, F. Jaouen, J.-P. Dodelet, Science 324 (2009) 71–74.
[10] E. Yeager, Electrochim. Acta 29 (1984) 1527–1537.
[11] K. Wiesener, Electrochim. Acta 31 (1986) 1073–1078.
[12] S. Maldonado, K.J. Stevenson, J. Phys. Chem. B 109 (2005) 4707–4716.
[13] P.H. Matter, L. Zhang, U.S. Ozkan, J. Catal. 239 (2006) 83–96.
[14] K.A. Kurak, A.B. Anderson, J. Phys. Chem. C 113 (2009) 6730–6734.
[15] N.P. Subramanian, S.P. Kumaraguru, H. Colon-Mercado, H. Kim, B.N. Popov, T. Black, D.A. Chen, J. Power Sources 157 (2006) 56–63.
[16] X. Li, H.R. Colon-Mercado, G. Wu, J.-W. Lee, B.N. Popov, Electrochem. Solid State Lett. 10 (2007) B201–B205.
[17] V. Nallathambi, J.-W. Lee, S.P. Kumaraguru, G. Wu, B.N. Popov, J. Power Sources 183 (2008) 34–42.
[18] X. Li, L. Liu, J.-W. Lee, B.N. Popov, J. Power Sources 182 (2008) 18–23.
[19] N. Subramanian, X. Li, V. Nallathambi, S. Kumaraguru, H. Colon-Mercado, G. Wu, J.-W. Lee, B.N. Popov, J. Power Sources 188 (2009) 38–44.
[20] G. Liu, X. Li, P. Ganesan, B.N. Popov, Appl. Catal. B 93 (2009) 156–165.
[21] X. Li, S. Park, B.N. Popov, J. Power Sources 195 (2010) 445–452.
[22] G. Liu, X. Li, P. Ganesan, B.N. Popov, Electrochim. Acta 55 (2010) 2853–2858.
[23] X. Li, G. Liu, B.N. Popov, J. Power Sources 195 (2010) 6373–6378.
[24] B.N. Popov, X. Li, G. Liu, Int. J. Hydrogen Energy (2010), doi:10.1016/j.ijhydene, 2009.12.050.
[25] P. Gouerec, M. Savy, Electrochim. Acta 44 (1999) 2653–2661.
[26] M. Lefevre, J.P. Dodelet, Electrochim. Acta 48 (2003) 2749–2760.
[27] H. Schulenburg, S. Stankov, V. Schu1nemann, J. Radnik, I. Dorbandt, S. Fiechter, P. Bogdanoff, H. Tributsch, J. Phys. Chem. B 107 (2003) 9034–9041.
[28] J. Maruyama, I. Abe, J. Electrochem. Soc. 154 (2007) B297–B304.
[29] E. Proietti, S. Ruggeri, J.P. Dodelet, J. Electrochem. Soc. 155 (2008) B340–B348.
[30] A. Garsuch, R. d'Eon, T. Dahn, O. Klepel, R.R. Garsuch, J.R. Dahn, J. Electrochem. Soc. 155 (2008) B236–B243.
[31] G. Wu, K. Artyushkova, M. Ferrandon, J. Kropf, D. Myers, P. Zelenay, ECS Trans. 25 (2009) 1299–1311.
[32] X. Li, C. Liu, W. Xing, T. Lu, J. Power Sources 193 (2009) 470–476.
[33] F. Charreteur, F. Jaouen, J.P. Dodelet, Electrochim. Acta 54 (2009) 6622–6630.
[34] S. Kundu, T.C. Nagaiah, W. Xia, Y. Wang, S. Van Dommele, J.H. Bitter, M. Santa, G. Grundmeier, M. Bron, W. Schuhmann, M. Muhler, J. Phys. Chem. C 113 (2009) 14302–14310.
[35] S.Lj. Gojkovic, S. Gupta, R.F. Savinell, J. Electroanal. Chem. 462 (1999) 63–72.
[36] M. Piana, S. Catanorchi, H.A. Gasteiger, ECS Trans. 16 (2008) 2045–2055.
[37] J. Herranz, F. Jaouen, J.-P. Dodelet, ECS Trans. 25 (2009) 117–128.
[38] K. Kinoshita, Carbon, in: Electrochemical and Physiochemical Properties, John Wiley & Sons, New York, 1988 (Chapter 6).